Evidence for compact binary systems around *Kepler* red giants

Isabel L. Colman[1,2]*, Daniel Huber[1,2,3,4], Timothy R. Bedding[1,2], James S. Kuszlewicz[2,5], Jie Yu[1,2], Paul G. Beck[6], Yvonne Elsworth[2,5], Rafael A. García[6], Steven D. Kawaler[7], Savita Mathur[8], Dennis Stello[1,2,9], and Timothy R. White[2]

[1] *Sydney Institute for Astronomy, School of Physics, A28, University of Sydney, NSW, 2006, Australia*
[2] *Stellar Astrophysics Centre, Department of Physics and Astronomy, Aarhus University, Ny Munkegade 120, DK-8000 Aarhus C, Denmark*
[3] *Institute for Astronomy, University of Hawai'i, 2680 Woodlawn Drive, Honolulu, HI 96822, USA*
[4] *SETI Institute, 189 Bernardo Avenue, Mountain View, CA 94043, USA*
[5] *School of Physics and Astronomy, University of Birmingham, Edgbaston, Birmingham B15 2TT, UK*
[6] *Laboratoire AIM, CEA/DRF - CNRS - Univ. Paris Diderot - IRFU/SAp, Centre de Saclay, 91191 Gif-sur-Yvette Cedex, France*
[7] *Department of Physics and Astronomy, Iowa State University, Ames, IA 50011, USA*
[8] *Center for Extrasolar Planetary Systems, Space Science Institute, 4750 Walnut street Suite 205, Boulder, CO 80301, USA*
[9] *School of Physics, University of New South Wales, NSW 2052, Australia*

ABSTRACT

We present an analysis of 168 oscillating red giants from NASA's *Kepler* mission that exhibit anomalous peaks in their Fourier amplitude spectra. These peaks result from ellipsoidal variations which are indicative of binary star systems, at frequencies such that the orbit of any stellar companion would be within the convective envelope of the red giant. Alternatively, the observed phenomenon may be due to a close binary orbiting a red giant in a triple system, or chance alignments of foreground or background binary systems contaminating the target pixel aperture. We identify 87 stars in the sample as chance alignments using a combination of pixel Fourier analysis and difference imaging. We find that in the remaining 81 cases the anomalous peaks are indistinguishable from the target star to within $4''$, suggesting a physical association. We examine a Galaxia model of the *Kepler* field of view to estimate background star counts and find that it is highly unlikely that all targets can be explained by chance alignments. From this, we conclude that these stars may comprise a population of physically associated systems.

Key words: stars: oscillations (including pulsations), (stars:) binaries (including multiple): close

1 INTRODUCTION

This paper sets out to solve a long-standing problem in the study of oscillating *Kepler* red giants. The analysis of red giants has been an area of rapid growth with the advent of data from the *Kepler* mission (Borucki et al. 2010). In particular, asteroseismology has allowed unprecedented insights into their core fusion (Bedding et al. 2011), internal rotation (Mosser et al. 2012; Beck et al. 2012), and internal magnetic fields (Stello et al. 2016). Red giants have also contributed to the field of galactic archaeology, where the study of red giant populations is used to map the formation history of the galaxy (Miglio et al. 2013; Casagrande et al. 2016).

The red giants in this study were first noted in the early days of *Kepler*. Initial analysis revealed anomalous high-amplitude peaks in their Fourier spectra. Figure 1 shows amplitude spectra using the first quarter of data and data from all quarters for the first star observed to exhibit this behaviour, KIC 4350501 (Bedding et al. 2010). Note that the heights of the oscillation modes in the amplitude spectrum decrease as the observing time is increased because the modes become more resolved.

These anomalous peaks were first suggested to be mixed modes (Bedding et al. 2010), which are caused by the coupling between p modes propagating in the convective enve-

* icol6407@uni.sydney.edu.au
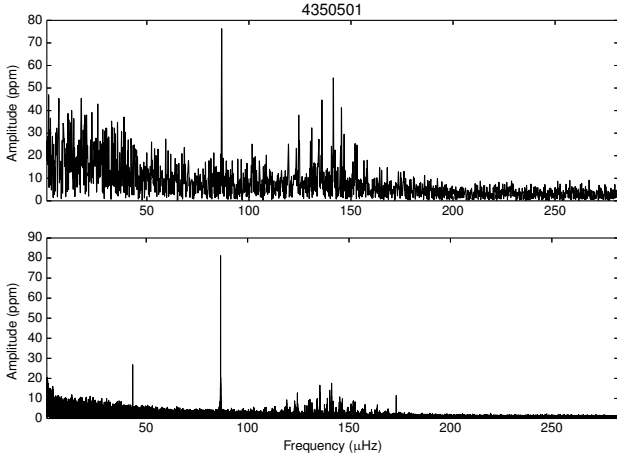
Figure 1. Top panel: Amplitude spectrum of KIC 4350501, the first noted red giant with an anomalous peak, using only 43 days of data (Q0 and Q1), as in Bedding et al. (2010). Bottom panel: Amplitude spectrum calculated using all four years of *Kepler* data. The oscillations are centred at $140\,\mu$Hz; the anomalous peak is at $\sim 86\,\mu$Hz.

lope with g modes propagating in the radiative core. Solar-like oscillations are stochastically excited and damped, with narrower peaks indicating longer mode lifetimes, as expected for mixed modes. **For a recent review of red giants and their oscillations, see Hekker & Christensen-Dalsgaard (2016).** In the case of KIC 4350501, more data showed the anomalous peak to be intrinsically narrow and revealed a subharmonic at half the frequency of the peak, suggesting that the peak was not a mixed mode but rather the signature of tidal interactions in a binary system. We have subsequently found many other red giants that show this type of behaviour, including the presence of harmonics and subharmonics. However, these peaks are present at such short periods that any binary companion would have to be orbiting within the convective envelope of the red giant.

This raises the possibility that we are observing common-envelope systems (Paczynski 1976). This is a phase of binary evolution that has been extensively studied with modelling and population synthesis. Evidence to confirm the existence of common-envelope systems is hard to come by; the closest method we have to direct detection is studying observational phenomena indicative of a past common-envelope phase. Recent studies have used the shaping of planetary nebulae with binary central stars to better understand common-envelope interaction (Hillwig et al. 2016), and jets in planetary nebulae to constrain the magnetic fields of common-envelope binaries (Tocknell et al. 2014). It has also been postulated that the common-envelope phase could be integral to the evolution of red giants into sdB stars and cataclysmic variables (Beck et al. 2014). The observation of a common-envelope system would provide important confirmation for these theories of binary evolution. For a recent review of our understanding of common-envelope systems, see Ivanova et al. (2013).

Another possibility is that these objects may be examples of hierarchical triple systems, where a compact binary orbits a red giant, e.g. "Trinity" (Derekas et al. 2011;

Fuller et al. 2013). These anomalous peaks could arise from a background or foreground compact binary that has contaminated the light collected from the red giant. **There is still a limit to our knowledge of hierarchical triple systems and common-envelope binaries. The Trinity system is the best-studied observational example of a hierarchical triple involving a red giant. The red giant in Trinity does not exhibit any oscillations, and it is expected that red giant oscillations would be suppressed by binarity, but we found no such trend in the stars in this study. Ultimately, we cannot extrapolate from the case of Trinity to the many possible cases in this study, so the population of triple systems remains a hypothesis.**

This study examines a sample of 168 light curves that exhibit both red giant oscillations and an anomalous peak, often with harmonics or a subharmonic. In this paper, we outline the method used to identify chance alignments, and comment on the statistics of possible physically associated systems.

## 2 METHODS AND ANALYSIS

2.1 Data preparation

The 168 stars studied were all discovered among *Kepler* red giants by visual inspection of power spectra. Many were included in Huber et al. (2010), Huber et al. (2011), or Stello et al. (2013). Additional stars were taken from Yu et al. (2016) or found in the APOKASC sample (Pinsonneault et al. 2014).

We began by downloading and preparing *Kepler* simple aperture photometry (SAP) light curves from MAST[1]. We processed the light curves following García et al. (2011), initially performing a high-pass filter using a Gaussian of width 100 days. We followed this by clipping all outliers further than 3σ from the mean. Finally, we took a Fourier transform to produce the amplitude spectrum.

We first located the comb-like pattern of solar-like oscillations, typical of red giant stars. Then, we were able to identify anomalous peaks. These have no particular position in relation to the solar-like oscillations. The majority of anomalous peaks had amplitudes higher than or comparable to the oscillations. Some anomalous peaks were found at similar frequencies to the oscillations, which led to a degree of confusion in stars that were identified previously with fewer quarters of data. A subset of the stars that we initially considered to fit this pattern were discarded from this study due to the anomalous peak representing an oscillatory $\ell = 0$ or $\ell = 2$ mode with a relatively broad peak, implying a shorter mode lifetime.

Using the frequency of the high-amplitude anomalous peak, we phase-folded each star's time series. The majority of the resulting phase curves displayed ellipsoidal variation, lending weight to the theory that these peaks are due to binarity. None of the anomalous peaks included in this study displayed the phase variation expected of a red giant oscillation. Examples are given in Figure 2. In some cases there were also subharmonics present in the Fourier spectra, as

---

[1] http://archive.stsci.edu/kepler/
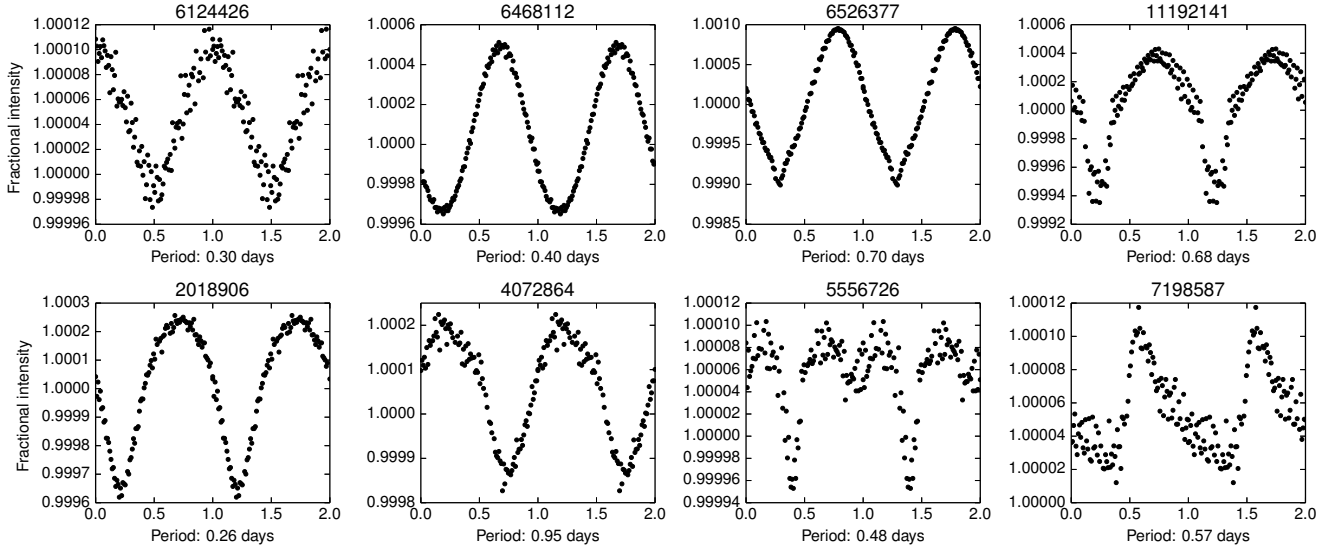
Figure 2. A variety of light curves phased on the period of the anomalous peak and binned. The top row shows stars that could not be discounted as chance alignments in this study. The bottom row shows chance alignments.
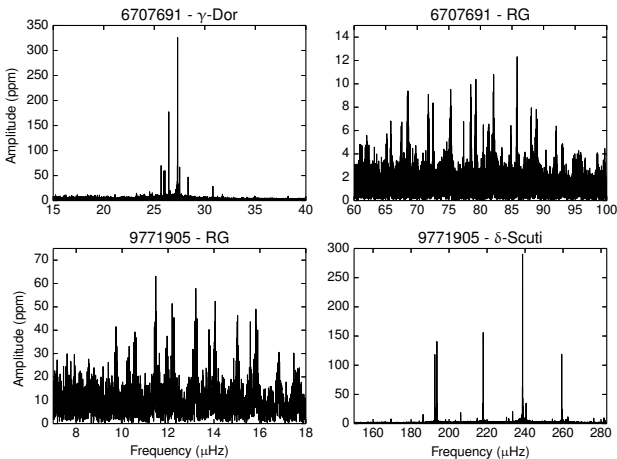
Figure 3. Top row: KIC 6707691, showing both γ-Dor (left) and red giant (right) oscillations. Bottom row: KIC 9771905, showing both red giant (left) and δ-Scuti (right) oscillations. Each set of oscillations is isolated to better display its features, as in each star the red giant oscillations have significantly lower amplitudes than the classical pulsator oscillations.

with KIC 4350501 (Figure 1), or a series of peaks indicative of an eclipse.

In two cases, we found the anomalous peaks to come from γ-Doradus oscillations and five stars where the source of the anomalous peaks are δ-Scuti pulsators, indicating possible binary systems. An example of red giants contaminated by γ-Dor and δ-Scuti oscillations is shown in Figure 3. Although these stars do not conform to the typical pattern of red giant oscillations with one anomalous peak and possible harmonics and subharmonics, we in-

clude them in this paper as they were studied with the same processes as the remainder of the sample and provide confirmation that the method works independently of what type of target it is used to analyse.

2.2 Pixel power spectrum analysis

In the previous section we covered the process of identifying stars for this sample. For this, we used SAP light curves, which are a composite of several $4''$ *Kepler* pixels comprising the so-called 'optimal aperture.' To locate the true sources of these anomalous peaks, it was necessary to examine the area around each of the targets. For this, we used *Kepler* target pixel files (TPFs), which are available for download from MAST. TPFs provide a 'postage stamp' image of pixels around *Kepler* targets. We employed the same methods outlined in Section 2.1 to process light curves from individual pixels in each TPF.

During the *Kepler* mission, the orientation of the telescope changed by $90°$ every quarter. Because of this, we examined each quarter of pixel data separately. In cases where oscillations were not visible with only one quarter of data, we stitched together the light curves of quarters with the same orientation, which occurred every fourth quarter.

By taking a Fourier transform of each pixel time series, we could more accurately locate the source of the anomalous peaks in the Fourier spectra. We identified these by inspection, based on the pixels included in the optimal aperture around the target star. In many cases, the source of the anomalous peak was obviously separated from the source of the solar-like oscillations. Figure 4 shows an example of such a TPF for KIC 7461601, where the optimal aperture is indicated by red shading. In this case, the anomalous peak is primarily located outside the optimal aperture. It is evident that its source is separate to the source of the oscillations. Of the 168 stars analysed, we found 87 to display this type
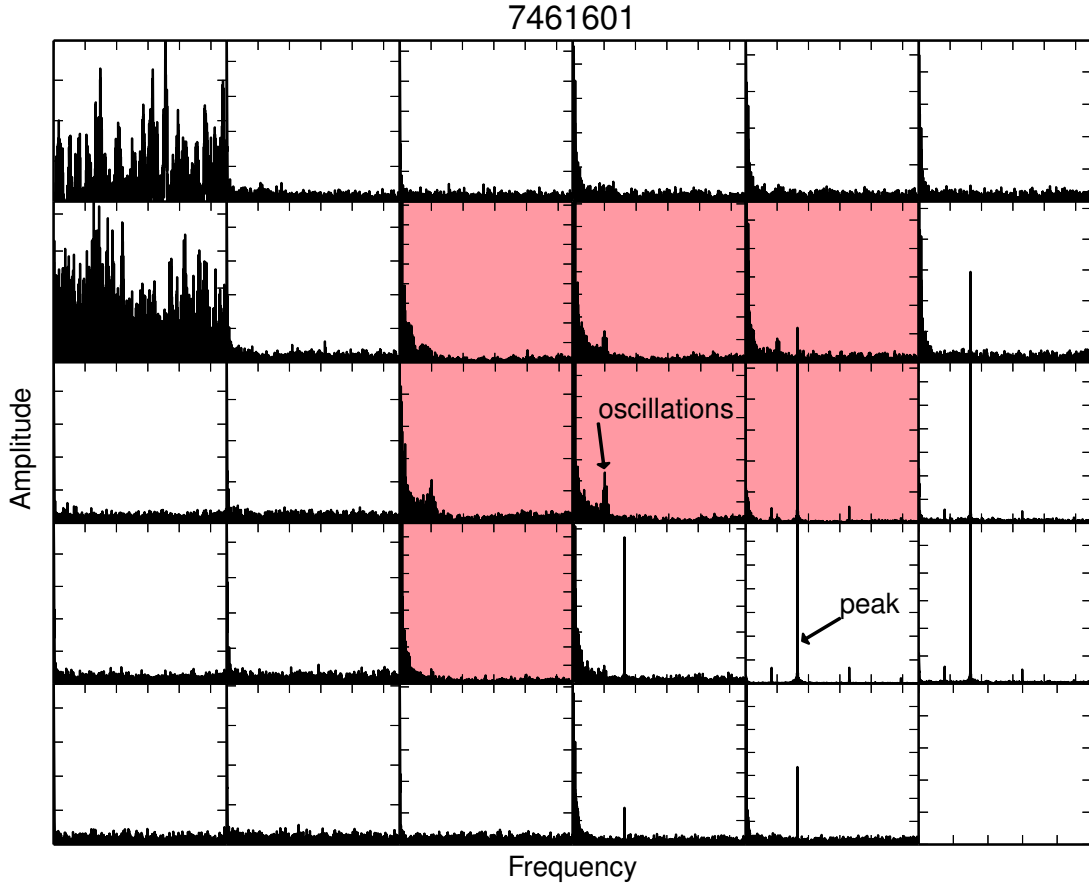
Figure 4. The *Kepler* TPF aperture of KIC 7461601, a red giant showing contamination from a chance alignment with a binary. Each panel represents a pixel, showing an amplitude spectrum calculated using the same methods as in Figure 1 with frequencies up to the *Kepler* long cadence Nyquist frequency, 283.21μHz. Amplitudes in each pixel are auto-scaled in order to better display qualitative features. More compact tick marks indicate higher overall amplitudes. Shaded pixels indicate the optimal aperture.

of clear separation. We interpret these as chance alignments of red giants with background or foreground binaries. The other 81 stars did not show this sort of clear separation. Figure 5 shows the TPF for KIC 3736251, a case where there is no clear distinction between the pixel source of the red giant oscillations and the anomalous peak. We interpret these as possibly physically associated systems.
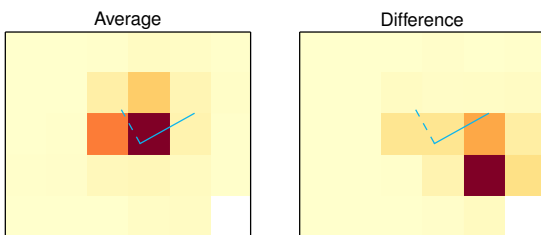
2.3 Difference imaging

We performed a more detailed study of the TPFs with difference imaging, which has been successfully applied to the identification of false positive exoplanet transits (Bryson et al. 2013). We selected postage stamp images that fell in time within 10% bands centred on the maximum and minimum points of the phased light curve. To create the difference image, we took the average of both sets of images and subtracted the average about the minima from the average about the maxima. This new image retained the dimensions of a TPF postage stamp and could easily be compared to the

average images, as shown in Figure 6. From this, we could see which pixels were the source of the flux variations at the period of the anomalous peak.

There remain some caveats for the use of difference imaging. The method we used was designed for ellipsoidal variation, and so it was less useful for the few stars in the sample where the phased light curve showed an eclipse, or where the identified anomalous peak belonged to δ-Scuti oscillations with multiple high-amplitude peaks. There were several other issues with using the phased light curves, particularly in stars with a low signal-to-noise ratio where the periodicity was hard to discern by looking at the phased light curve, due to scatter. Additionally, difference imaging was less successful for cases where the contaminant was at an angular distance greater than $30''$ from the target star. Some stars with clear contamination in the TPF did not show any variation in the difference image, which suggested that the contaminant was located outside the optimal aperture. This tended to coincide with low-amplitude anomalous
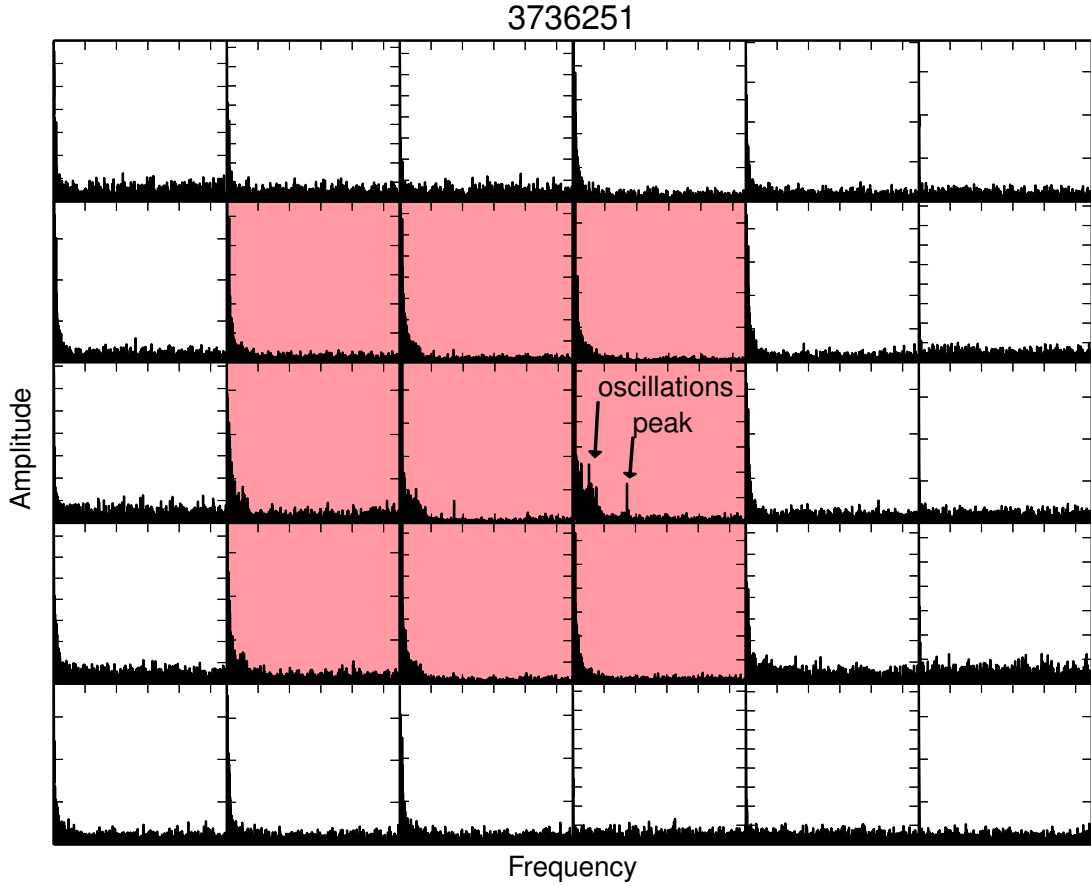
Figure 5. The *Kepler* TPF aperture of KIC 3736251, showing no contamination. Each panel represents a pixel, as in Figure 4.
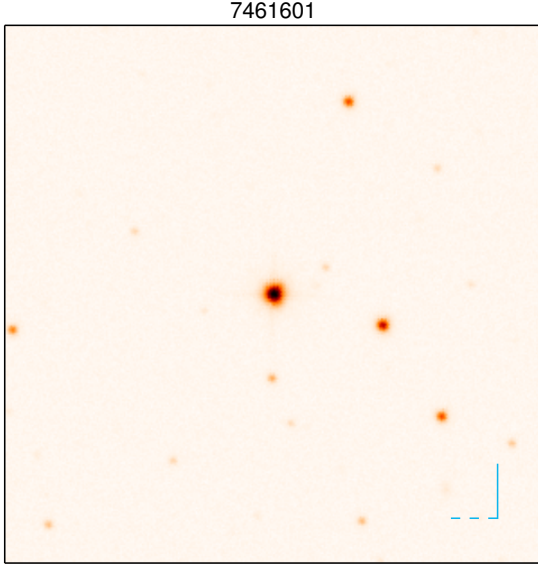

Figure 6. An example of difference imaging, displaying the KIC 7461601 aperture as in Figure 4. To indicate scale, the compass arms are 6″. The solid line points north, and the dashed line points east. The variation originating from the bottom right corner of the TPF can be clearly seen in the difference image.

peaks. In such cases, it was clear simply from the TPFs that there was contamination.

Despite this, we were still able to gain valuable information from difference imaging. For stars with no evident contamination in the TPFs, the difference images tended not to show variation when compared to the average im-

ages. Difference imaging also helped to confirm the status of stars with low signal in the TPF Fourier spectra. Conversely, the difference images reinforced the status of stars with more tentative classification as spatially separated. It follows that many of the cases where difference imaging did not confirm contamination correspond to widely separated chance alignments.

To identify the true source of chance alignments, widely-separated or otherwise, we next compared both the average and difference images to higher-resolution images of the same area of sky, using 1′ cutouts from the UKIRT WF-CAM (the UK Infrared Telescope Wide Field Camera) survey (Lawrence et al. 2007). An example is shown in Figure 7. *Kepler* TPFs contain world coordinate system (WCS) information, which allowed us to calculate the orientation of the postage stamp. We displayed coordinates on both types of images in the form of a compass rose, from which we could see whether there were any possible contaminant stars from the same position as the anomalous source as shown in the TPF Fourier spectra. Looking for matches in both the KIC and the UKIRT object catalogue, we were able to use a *Kepler* light curve to confirm the source of contamination in 18 cases (see Table 2 in the appendix.) For 87 of the other

Figure 7. A UKIRT image showing a 1′ field of view around KIC 7461601. To indicate scale, the compass arms are 6″, as in Figure 6. The solid line points north, and the dashed line points east.

chance alignments (Table 4), we noted one or more possible stars that could be the contaminant, especially closer to the Galactic plane, which is where most of the chance alignments were found.

3   DISCUSSION

3.1   Spatial distribution

We found that, of the 168 red giants with anomalous peaks, 87 could be identified as chance alignments. For 18 of these chance alignments, we confirmed their status with the analysis of *Kepler* light curves of nearby stars which we identified as the sources of contamination. We could not spatially resolve the 81 other stars, and we refer to these as possibly associated systems. **We identified four of the five δ-Scuti anomalous peaks as chance alignments. The two γ-Dor anomalous peaks remain possible physical associations.**

Figure 8 shows the distribution of our sample over the *Kepler* field of view (FOV), with chance alignments in panel (a) and possibly associated systems in panel (b). We present these populations in galactic coordinates, and note that the bottom of the field at lower galactic latitudes is closer to the Galactic plane and has a higher density of stars. At higher galactic latitudes we observe a marked paucity of stars as expected, both in the field itself and in the sample considered in this study. Similarly, this pattern presents itself in the distribution of chance alignments. It is therefore noteworthy that the possibly associated systems seen in panel (b) seem to be spread quite evenly across the FOV.

We further analysed these populations by examining

their cumulative distributions as a function of galactic latitude, shown in Figure 9. We compare this to a distribution of 1,000 red giants drawn randomly from a list of all oscillating *Kepler* red giants provided from Yu et al. (in preparation). The distribution of the possible physical associations closely matches the distribution of random red giants, which implies that they are not chance alignments. It is also noteworthy that these distributions visibly differ from the distribution of chance alignments, which increases sharply at low galactic latitudes, reflecting the higher density of stars closer to the Galactic plane. The probability of finding a chance alignment between two populations is expected to scale as the square of surface density. This gives us an important insight into the nature of this population and suggests that we may be observing a distinct population of systems, possibly hierarchical triples or common envelope binaries.
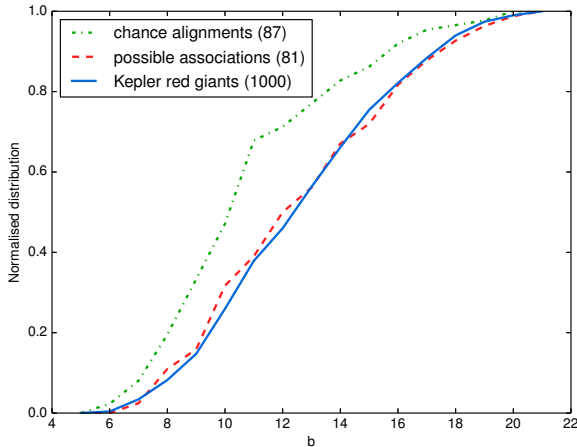
3.2   Amplitude distribution

We searched for a possible correlation between the intrinsic luminosities of the red giants and the amplitudes of their anomalous peaks. It might be expected that if a compact binary is physically associated with a red giant, the amplitude of variations from the binary might correlate inversely with the luminosity of the red giant, due to dilution. We observed no correlation, which led us to compare our stars to a sample drawn from the *Kepler* Eclipsing Binary Catalog (Prša et al. 2011)[2]. We selected the sample of eclipsing binaries (EBs) by their morphology, which is a measure of the ellipticity of their phased light curves calculated by locally linear embedding (Matijevič et al. 2012). The cut off for EB selection was a morphology number > 0.7, chosen by visual inspection of stars in the catalog to match those with light curves similar to those in our sample. In Figure 10, we plot the amplitudes of the anomalous peaks in our sample and of the *Kepler* EBs against *Kepler* magnitude. These data show that more ellipsoidal variation tends to have a lower amplitude of variation, a trend which is also present in our sample. The measure of ellipticity in our data was based on a ranking of the shape of phased light curves and on a different scale to the Catalog's morphology number, so we do not display it in Figure 10.

From this exercise, we can explain the lack of correlation between the intrinsic luminosities of red giants and the amplitudes of their anomalous peaks by the broad range of amplitudes present across ellipsoidal variables, as exhibited by the Catalog sample. We also note that while our sample is overall brighter than the Catalog sample, the distribution of amplitudes is what would be expected for a sample primarily exhibiting ellipsoidal variation. The histogram in the right panel of Figure 10 shows that the distribution of the possible physical associations closely matches the distribution of the Catalog EBs. The anomalous peaks of both the possible physical associations and the chance alignments are more present at lower amplitudes, but this is markedly noticeable for the latter. This effect can be explained by the wide angular separation between the target stars and their contaminants, so less of the contaminating light enters the

---

[2] `http://keplerebs.villanova.edu/`
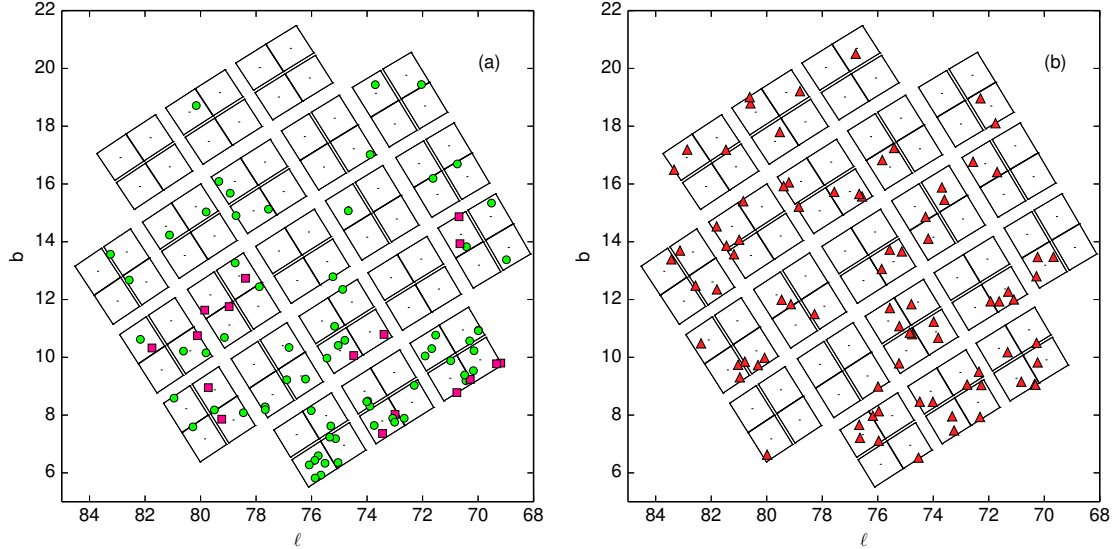
Figure 8. The sample of stars in this study is shown across the *Kepler* field of view in galactic coordinates. Panel (a) shows red giants with anomalous peaks that we classified as chance alignments, shown as green circles. In the case where a *Kepler* light curve was available to confirm this contamination, the star is shown by a pink square. Panel (b) shows the population of red giants exhibiting an anomalous peak and where a physical separation cannot be discerned.

Figure 9. Cumulative distributions in galactic latitude of the populations shown in panels (a) and (b) of Figure 8. The solid blue line is taken from a random sample of 1,000 *Kepler* red giants.

optimal aperture. This leads to systematically lower apertures. In the case of the possible physical associations, this dilution could be caused by a compact binary companion. This strengthens the conclusion that the possible physical associations comprise a distinct population.

3.3 Modelling of chance alignments

While the majority of chance alignments found in this study involved contaminants further than $4''$ from the target star,

it is possible that there could be contaminants within $4''$ of the target that our methods do not have the sensitivity to detect. To test whether we could expect to find more chance alignments within the remaining 81 stars, we analysed a model of a stellar population in the *Kepler* FOV. This also helped us in understanding the underlying statistics around chance alignments of red giants and background or foreground binary systems.

We used the modelling software Galaxia (Sharma et al. 2011), which allows the user to synthesise an artificial population of stars within a given area of sky, here chosen to match the *Kepler* FOV. We defined a chance alignment as any two stars found within a *Kepler* pixel of each other, namely $4''$. Galaxia does not take into account the existence of binary systems, and hence any chance alignments that are detected in the simulation are true chance alignments.

Our model goes down to an apparent J magnitude of 20. Once the synthetic FOV had been simulated, we then searched for stars analogous to those in the sample by minimising over apparent J magnitude within a set range of galactic coordinates b and ℓ, and stellar parameters $T_{\rm eff}$, $\log(g)$ and [Fe/H] (Mathur et al. 2016). The nearest match to each target star was designated a blend if we located another star within $4''$ of it. This process is illustrated in Figure 11.

We found the occurrence of $4''$ chance alignments in the model to be rare, with only 18 of 168 these stars fitting the criterion, or 10.7%. This is much lower than the observed fraction (as discussed in Section 3.1) because here we are only looking at matches within $4''$, which cannot be discerned by the techniques covered in Section 2. This can be compared with the figure quoted in a study of false positive KOIs (*Kepler* Objects of Interest) by Ziegler et al. (2016), who found that planet host candidates have a nearby star
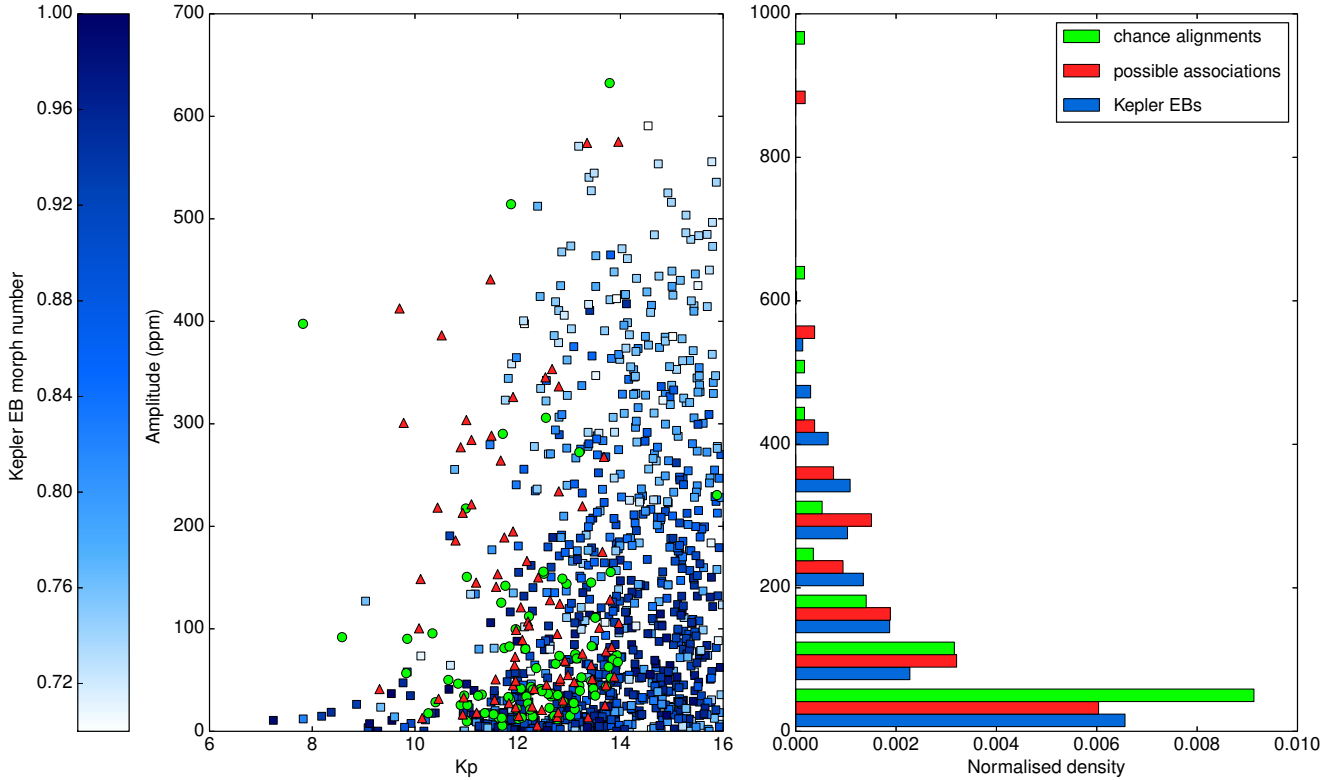
Figure 10. Left: Relationship between the amplitude of the anomalous peaks in our sample and *Kepler* magnitude. Chance alignments are shown with green circles, and possible physical associations with red triangles. For comparison, we also display the amplitudes of a population selected from the *Kepler* Eclipsing Binary Catalog with morphology number > 0.7, shown with blue squares. Right: Histogram of each population distributed across amplitude. Not pictured: two outliers with amplitudes above 700ppm, one chance alignment (KIC 4071950) and one possible physical association (KIC 6526377).

within $0.15'' - 4''$ with a probability of $12.6\% \pm 0.9$. Despite the fact that Ziegler et al. were not focused on red giants in the same way as our study, our value is just over 2σ from the result given by Ziegler et al., which places the two samples in good agreement. This suggests that a similar proportion of our sample will contain chance alignments within $4''$. By inspection of UKIRT images, 9 of the identified chance alignments appear to be close to or within $4''$. This implies that we should expect to find roughly 9 more chance alignments within $4''$ among the 81 stars that have not been identified as chance alignments. This is a strong result, and leaves us with a sizeable population of possible physical associations involving an oscillating red giant.

4 CONCLUSIONS

From a sample of 168 red giant stars with anomalous high-amplitude peaks, we found 87 could be discounted as chance alignments, with the remaining 81 exhibiting no contamination outside a *Kepler* pixel. This leaves the opportunity for these stars to be physically associated systems such as a common-envelope binary or hierarchical triple systems. We observe that this population appears to follow the distribution of randomly-selected stars from the *Kepler* FOV. This distinguishes them from the population of chance alignments, which appear with a greater density towards the

galactic plane. We have constructed and examined a model of a synthetic population in the *Kepler* field which suggests that such close chance alignments are rare, which would imply that most of these stars are more likely to be physically associated systems. This may point to hierarchical triple systems, or to common-envelope binaries.

Future work includes an observation of all remaining targets by Robo-AO (Baranec et al. 2011), an adaptive optics system which has been used previously to examine *Kepler* exoplanet host candidates. We will also look to spectroscopic follow-up observations, with the possibility of identifying the spectral lines of companion stars or radial velocity variations. In addition to this, further opportunities will arise to search for these unusual red giants in data from K2 and TESS. A larger sample from different areas of the sky would aid our understanding of these unusual cases and aid more detailed analysis of a possible new population of systems.

The fundamental parameters of the stars in this study are listed in tables in the appendix. All code used for analysis is available online at `https://github.com/astrobel/chancealignments`.
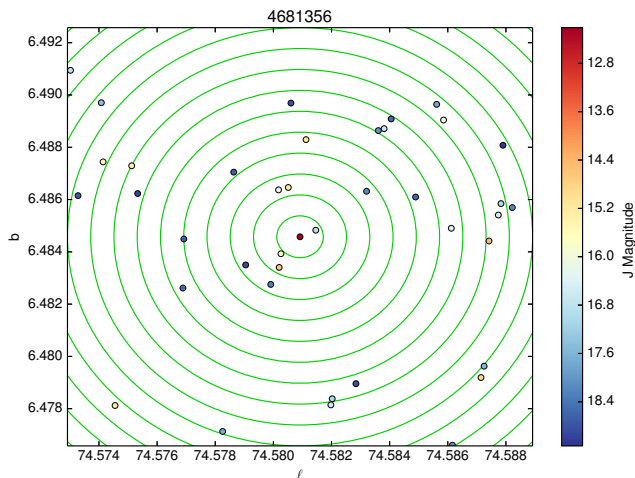
Figure 11. An illustration of the process used to search for chance alignments in the Galaxia model, described in Section 3.3. The concentric rings have radius $4''$, intended to represent the maximum distance between stars that could fall on the same *Kepler* pixel. The colour scale represents J magnitude.

REFERENCES

Baranec C. et al., 2011, eprint: arXiv:1212.0825
Beck P. G. et al., 2014, Astronomy and Astrophysics, 564, A36
Beck P. G. et al., 2012, Nature, 481, 55
Bedding T. R. et al., 2010, The Astrophysical Journal Letters, 713, L176
Bedding T. R. et al., 2011, Nature, 471, 608
Borucki W. J. et al., 2010, Science, 327, 977
Bryson S. T. et al., 2013, Publications of the Astronomical Society of the Pacific, 125, 889
Casagrande L. et al., 2016, Monthly Notices of the Royal Astronomical Society, 455, 987
Casali M. et al., 2007, Astronomy and Astrophysics, 467, 777
Derekas A. et al., 2011, Science, 332, 216
Fuller J., Derekas A., Borkovits T., Huber D., Bedding T. R., Kiss L. L., 2013, Monthly Notices of the Royal Astronomical Society, 429, 2425
García R. A. et al., 2011, Monthly Notices of the Royal Astronomical Society, 414, L6
Hambly N. C. et al., 2008, Monthly Notices of the Royal Astronomical Society, 384, 637
Hekker S., Christensen-Dalsgaard J., 2016, ArXiv e-prints, 1609, arXiv:1609.07487
Hewett P. C., Warren S. J., Leggett S. K., Hodgkin S. T., 2006, Monthly Notices of the Royal Astronomical Society, 367, 454
Hillwig T., Jones D., De Marco O., Bond H., Margheim S., Frew D., 2016, ArXiv e-prints, 1609, arXiv:1609.02185
Huber D. et al., 2011, The Astrophysical Journal, 743, 143
Huber D. et al., 2010, The Astrophysical Journal, 723, 1607
Ivanova N. et al., 2013, Astronomy and Astrophysics Review, 21, 59
Lawrence A. et al., 2007, Monthly Notices of the Royal Astronomical Society, 379, 1599
Mathur S. et al., 2016, ArXiv e-prints, 1609, arXiv:1609.04128
Matijevič G., Prša A., Orosz J. A., Welsh W. F., Bloemen S., Barclay T., 2012, The Astronomical Journal, 143, 123
Miglio A. et al., 2013, Monthly Notices of the Royal Astronomical Society, 429, 423
Mosser B. et al., 2012, Astronomy and Astrophysics, 548, A10
Paczynski B., 1976, in Structure and Evolution of Close Binary Systems; Proceedings of the Symposium, Vol. 73, D. Reidel Publishing Co., Cambridge, England, p. 75
Pinsonneault M. H. et al., 2014, The Astrophysical Journal Supplement Series, 215, 19
Prša A. et al., 2011, The Astronomical Journal, 141, 83
Sharma S., Bland-Hawthorn J., Johnston K. V., Binney J., 2011, The Astrophysical Journal, 730, 3
Stello D., Cantiello M., Fuller J., Huber D., García R. A., Bedding T. R., Bildsten L., Aguirre V. S., 2016, Nature, 529, 364
Stello D. et al., 2013, The Astrophysical Journal Letters, 765, L41
Tocknell J., De Marco O., Wardle M., 2014, Monthly Notices of the Royal Astronomical Society, 439, 2014
Warren S. J. et al., 2007, arXiv:astro-ph/0703037, arXiv:astro-ph/0703037

Yu J., Huber D., Bedding T. R., Stello D., Murphy S. J., Xiang M., Bi S., Li T., 2016, Monthly Notices of the Royal Astronomical Society, 463, 1297

Ziegler C. et al., 2016, ArXiv e-prints, 1605, arXiv:1605.03584

Table 1. Details of the 81 possible physical associations. Stellar parameters are taken from the NASA Exoplanet Archive, data release 25 (Mathur et al. 2016). In cases where we found the anomalous peak to be part of γ-Dor oscillations, the peak frequency (ν_{peak}) is marked with an asterisk. We mark δ-Scuti anomalous peaks with two asterisks.

KIC	RA (deg)	DEC (deg)	Kp	log(g)	T_{eff} (K)	[Fe/H]	ν_{max} (μHz)	ν_{peak} (μHz)	P_{peak} (days)
1726211	292.50447	37.29278	10.93	2.39	4981	-0.74	31.56	66.01	0.18
1726245	292.51086	37.25521	11.57	2.59	4837	0.21	53.66	43.78	0.26
2160901	291.5993895	37.53966	12.06	2.67	4676	0.24	56.54	2.97	3.89
2449020	292.68245	37.75239	11.91	2.84	5007	0.07	66.76	13.98	0.83
2573092	290.85716	37.87599	11.58	2.46	4723	0.07	31.68	44.69	0.26
3356438	294.92994	38.47866	11.97	2.85	4999	0.07	58.40	5.94	1.95
3530823	287.101181	38.60348	11.74	2.56	5036	0.07	44.55	21.27	0.54
3546046	291.8050695	38.64798	11.96	3.18	4845	0.16	186.12	7.71	1.50
3736251	288.20211	38.8702	13.59	3.38	5148	-0.72	25.97	85.71	0.14
3858714	293.65017	38.95757	11.94	2.61	4852	0.21	48.27	61.02	0.19
3973137	296.026121	39.0659	13.65	2.41	4926	-0.58	36.93	2.56	4.53
4043436	287.40072	39.10863	12.77	2.42	4653	0.10	31.36	15.61	0.74
4149966	289.5747495	39.25492	10.08	2.79	4934	0.07	72.19	5.02	2.30
4164236	293.17628	39.24902	13.97	2.47	4738	-0.04	35.29	61.29	0.19
4279165	295.51473	39.36227	12.38	2.61	4868	-0.16	46.14	222.12	0.05
4374169	293.93991	39.41256	11.67	2.67	4891	0.07	40.07	7.83	1.48
4456739	289.362849	39.54505	12.02	2.44	4658	0.36	41.78	61.63	0.19
4555699	289.94031	39.69181	12.80	2.57	4768	-0.08	26.92	2.63	4.40
4681356	297.897023	39.709683	13.45	2.57	4710	-0.36	47.16	63.68	0.18
4830095	290.10768	39.96584	13.10	2.45	5166	-0.50	30.92	53.11	0.22
5112950	295.37307	40.20586	12.77	2.53	4753	0.00	41.51	91.43	0.13
5462460	295.65894	40.62042	12.40	2.41	4999	-0.50	32.70	40.99	0.28
5793628	292.67057	41.06844	11.10	2.48	4878	-0.48	36.04	49.55	0.23
5985252	298.17206	41.23463	11.00	2.31	4936	-0.50	27.47	37.37	0.31
6124426	292.1016	41.46219	13.88	3.68	5406	-0.28	205.92	39.16	0.30
6185964	284.57787	41.55982	12.98	2.65	4852	-0.42	27.75	39.86	0.29
6382801	296.9842395	41.73708	13.72	2.68	4724	0.28	38.10	69.47	0.17
6451664	294.57057	41.89605	12.56	2.45	4996	0.07	35.19	50.16	0.23
6462755	297.30729	41.84648	10.44	2.53	4785	-0.16	27.53	32.96	0.35
6468112	298.50825	41.8638	9.70	3.06	5089	-0.04	64.40	*29.22	0.40
6526377	293.07981	41.94772	11.81	2.59	4789	0.00	32.30	16.59	0.70
6610354	293.0651805	42.04949	9.31	2.61	4883	-0.20	45.46	7.74	1.50
6707691	295.9976805	42.17442	11.91	2.89	5122	0.07	85.82	*27.31	0.42
6716840	298.00289	42.11263	11.91	2.55	4841	0.36	27.57	40.50	0.29
6753216	282.487031	42.22581	11.49	3.34	5149	-0.74	46.87	**245.20	0.05
6929104	284.55087	42.46167	13.80	2.96	5054	-0.22	23.77	41.97	0.28
6948654	291.84099	42.43724	13.96	3.08	5048	0.10	32.78	36.40	0.32
6952430	293.019909	42.47953	11.83	2.48	4784	0.07	36.22	61.48	0.19
7267370	286.715829	42.88117	12.32	2.56	4835	0.07	43.74	61.69	0.19
7272332	288.70806	42.86038	13.26	2.63	4779	-0.14	46.89	58.60	0.20
7418275	281.62991	43.00333	13.37	3.41	5369	-0.10	221.62	57.55	0.20
7447072	292.4606	43.05733	13.26	2.93	5059	-0.16	33.26	23.22	0.50
7511777	286.22405	43.12891	13.72	3.53	5140	0.08	221.24	12.05	0.96
7596350	287.81166	43.25247	11.10	2.58	5153	-0.50	39.24	43.92	0.26
7816294	289.78314	43.52288	11.47	2.62	4644	0.18	48.01	25.45	0.45
8092097	289.94732	43.93543	12.80	2.43	4781	-0.20	24.50	33.33	0.35
8095225	290.95461	43.9071	13.43	3.32	5268	-0.04	79.96	76.07	0.15
8462775	301.53743	44.40842	10.89	2.68	4828	0.02	33.92	52.81	0.22
8870432	285.3189	45.1689	9.78	2.53	4733	0.56	35.00	45.39	0.25
9008090	286.0825605	45.3942	12.79	2.49	4785	0.07	38.46	67.39	0.17
9029195	294.38823	45.33999	10.93	2.52	4848	0.21	40.43	11.68	0.99
9146423	288.12324	45.55873	10.95	2.15	4499	-0.02	18.73	54.12	0.21
9210116	288.06693	45.68367	10.11	2.75	4912	0.07	53.87	43.65	0.27
9541892	297.49509	46.18827	12.67	2.54	4809	0.07	34.31	35.88	0.32
9605626	297.981431	46.26839	13.83	3.06	5122	-0.38	33.35	48.30	0.24
9763419	288.4587	46.50697	11.55	2.41	4934	0.07	32.20	49.54	0.23
9777198	294.5120895	46.59932	12.63	2.48	4775	0.21	36.39	40.76	0.28
9851743	298.97724	46.61877	10.46	2.54	4869	0.07	44.81	60.31	0.19
9908646	298.160649	46.73501	13.68	2.97	5021	-0.14	23.58	40.08	0.29
9969574	298.46844	46.88932	12.09	2.96	4812	0.30	108.63	4.00	2.90

KIC	RA (deg)	DEC (deg)	Kp	log(g)	T_{eff} (K)	[Fe/H]	ν_{max} (μHz)	ν_{peak} (μHz)	P_{peak} (days)
10334585	289.86435	47.43528	12.82	2.42	5023	-0.50	31.14	51.69	0.22
10384595	281.514071	47.50767	12.20	2.87	5186	0.07	44.83	55.09	0.21
10724041	288.92067	48.08529	12.28	2.41	4847	0.21	28.08	75.24	0.15
10855512	289.20384	48.20114	12.88	2.72	4724	0.00	65.23	12.09	0.96
10936814	298.47315	48.39799	10.79	2.47	4922	0.07	38.30	2.60	4.45
11140831	293.52471	48.79779	12.83	2.45	4862	-0.38	32.48	42.32	0.27
11145672	295.58421	48.79117	11.95	2.69	4915	-0.16	58.86	29.96	0.39
11177729	284.270741	48.87462	11.61	2.45	4896	0.07	32.84	42.99	0.27
11192141	292.719624	48.852017	10.52	2.01	4283	0.00	9.13	17.10	0.68
11287896	286.655441	49.03027	12.92	2.42	4947	0.07	34.53	55.10	0.21
11353223	293.29443	49.16571	12.47	2.63	4620	0.16	50.02	81.24	0.14
11400880	290.779849	49.27629	12.82	2.64	4755	-0.04	50.42	18.37	0.63
11567797	295.93539	49.51963	13.35	2.41	4816	0.07	30.69	5.60	2.07
11663151	292.58886	49.76146	11.96	2.68	4887	-0.24	36.30	47.11	0.25
11953849	285.76821	50.31719	11.20	2.45	4896	0.07	33.78	84.45	0.14
12003253	285.4657995	50.41648	11.19	2.41	4785	-0.24	34.27	4.48	2.58
12056767	288.59802	50.52476	10.14	2.45	4817	0.07	37.02	58.15	0.20
12067693	294.63153	50.55264	12.22	2.72	4862	0.36	29.97	65.34	0.18
12117920	295.27409	50.68874	12.18	2.45	4996	0.07	39.41	27.16	0.43
12645236	289.38545	51.76019	12.54	3.17	5114	-0.40	40.33	32.65	0.35
12737382	290.70515	51.90956	13.70	3.54	5023	-0.34	191.43	46.30	0.25

Table 2. Details of the 18 confirmed chance alignments with a known entry in the KIC. In cases where we found the anomalous peak to be part of δ-Scuti oscillations, the peak frequency (ν_{peak}) is marked with two asterisks.

KIC	RA (deg)	DEC (deg)	Kp	log(g)	T_{eff} (K)	[Fe/H]	ν_{max} (μHz)	ν_{peak} (μHz)	P_{peak} (days)	Contam. KIC
757076	291.03872	36.59813	11.68	3.58	5160	-0.10	271.50	31.86	0.36	757099
1026473	291.14901	36.72203	13.79	2.36	4788	-0.32	30.96	7.41	1.56	1026474
1872166	292.2872805	37.31746	11.63	2.82	4971	0.21	77.96	36.06	0.32	1872192
1872210	292.29633	37.31521	10.40	2.79	5250	0.21	78.82	17.28	0.67	1872192
2167774	293.07089	37.52352	9.85	2.69	4720	0.12	61.69	32.77	0.35	2167783
4071950	295.24143	39.11102	13.59	3.25	5004	-0.04	207.74	23.42	0.49	4071949
4077044	296.26499	39.18323	13.72	2.70	4832	-0.06	58.85	**167.62	0.07	4077032
4547321	287.067369	39.66424	13.93	3.18	4927	-0.04	245.22	40.12	0.29	4547308
4906950	285.9681405	40.06682	10.65	2.61	4655	0.14	52.14	18.80	0.62	4906947
5535029	292.2791805	40.74402	12.25	2.04	4462	-0.18	13.23	49.95	0.23	5535061
6048862	293.79036	41.3675	12.77	2.49	4941	0.07	34.46	86.85	0.13	6048876
8456004	299.5297905	44.40994	13.95	2.24	4562	-0.10	17.66	85.77	0.13	8456010
9045025	298.5382605	45.37306	12.47	2.66	4569	0.22	58.19	**164.00	0.07	9045002
9406638	292.86609	45.98426	11.36	2.49	4935	-0.50	39.83	90.95	0.13	9406652
9471796	294.5013705	46.06111	11.98	2.99	5014	0.21	103.73	12.53	0.92	9471797
9782817	296.54586	46.58502	11.84	2.61	4903	-0.32	53.07	80.03	0.14	9782831
9899421	295.23249	46.77037	12.30	2.32	4601	-0.22	26.00	34.74	0.33	9899414
10553525	298.23522	47.79192	12.81	2.80	4770	-0.26	76.44	16.24	0.71	10553491

Table 3. Details of the 69 presumed chance alignments. In cases where we found the anomalous peak to be part of δ-Scuti oscillations, the peak frequency (ν_{peak}) is marked with two asterisks.

KIC	RA (deg)	DEC (deg)	log(g)	Kp	T_{eff} (K)	[Fe/H]	ν_{max} (μHz)	ν_{peak} (μHz)	P_{peak} (days)
1870196	291.8805	37.34748	12.65	3.20	4895	0.10	191.59	60.77	0.19
2018906	292.42326	37.428	13.20	3.30	5046	-0.54	155.70	44.07	0.26
2163856	292.22694	37.55744	11.70	2.78	5010	0.07	72.14	144.29	0.08
2301349	291.09195	37.64004	13.43	2.72	4615	0.36	64.62	33.95	0.34
2569650	290.19609	37.81097	15.88	3.62	4986	0.22	187.60	74.04	0.16
2569935	290.222441	37.80783	13.12	1.55	4082	0.36	5.21	71.10	0.16
2696115	286.8690795	37.95218	11.85	2.19	4619	0.21	20.41	42.07	0.28
2710194	290.79134	37.92911	12.15	2.68	4580	0.24	54.74	33.60	0.34

KIC	RA (deg)	DEC (deg)	log(g)	Kp	$T_{\rm eff}$ (K)	[Fe/H]	$\nu_{\rm max}$ (μHz)	$\nu_{\rm peak}$ (μHz)	$P_{\rm peak}$ (days)
3118806	291.95328	38.21967	10.99	2.18	4569	0.36	18.05	57.58	0.20
3660820	295.19049	38.76184	11.87	2.40	4969	0.07	31.36	69.17	0.17
3858850	293.68329	38.98237	12.01	2.31	4523	0.36	20.33	83.69	0.14
3866844	295.5547695	38.99418	12.65	2.42	4710	0.36	33.33	64.32	0.18
3953330	291.242981	39.09661	12.55	2.28	4627	-0.44	16.58	6.30	1.84
3955590	291.86157	39.01267	10.34	2.19	4673	0.21	97.25	21.22	0.55
4059983	292.2911	39.10751	13.44	2.83	4842	0.56	31.96	51.18	0.23
4072864	295.445499	39.12097	13.81	3.34	4961	-0.06	183.22	12.17	0.95
4136374	284.8337805	39.21037	10.84	2.62	4876	0.07	48.53	7.32	1.58
4350501	287.07155	39.41622	11.74	3.06	5016	-0.22	141.40	86.65	0.13
4482738	296.13902	39.57963	12.95	3.06	4936	-0.44	141.34	53.44	0.22
4937770	295.47659	40.03605	13.15	2.90	4924	-0.32	91.11	63.60	0.18
4951617	298.4266905	40.06777	10.89	2.68	4822	0.04	43.31	110.44	0.10
5024414	295.316379	40.18652	12.71	2.81	5000	0.07	71.39	147.05	0.08
5112880	295.362821	40.20787	12.29	2.30	4501	0.10	27.71	66.38	0.17
5219666	299.3242695	40.37239	12.59	2.64	4665	0.36	56.52	29.74	0.39
5304555	298.761761	40.45563	12.78	2.56	4840	0.21	46.76	75.55	0.15
5308777	299.5773105	40.49851	13.20	2.84	4877	0.14	86.42	12.25	0.94
5385245	297.54492	40.55547	10.96	3.08	5083	-0.14	124.83	6.83	1.70
5556726	297.62054	40.76302	12.17	3.21	4898	0.07	207.26	24.04	0.48
5561523	298.632431	40.79503	13.47	2.99	4948	-0.06	34.49	73.03	0.16
5598645	283.7800305	40.81878	11.69	3.21	4973	-0.14	261.85	17.84	0.65
5648894	298.88994	40.82022	8.58	2.81	5068	-0.36	74.87	30.16	0.38
5725960	297.1535	40.92263	12.26	3.45	5171	-0.28	242.25	67.00	0.17
5736093	299.20563	40.91081	13.02	2.93	5121	0.07	106.57	50.05	0.23
6105113	284.81205	41.41103	13.24	3.10	4754	-0.02	32.89	52.65	0.22
6382830	296.992239	41.7899	11.01	2.24	4716	0.21	22.17	56.83	0.20
6447614	293.355371	41.88883	13.85	3.47	5132	-0.64	27.02	85.11	0.14
6612644	293.71154	42.01754	12.51	2.60	4681	0.28	44.85	18.77	0.62
6701238	294.48732	42.16711	11.30	2.40	4777	-0.30	27.26	97.46	0.12
6952355	292.99371	42.43124	13.11	2.98	4864	0.00	118.39	27.38	0.42
6963285	295.8375	42.49793	13.51	2.75	5102	0.21	181.09	57.55	0.20
7198587	291.2658405	42.73949	12.89	3.18	4968	0.18	168.98	20.42	0.57
7335713	280.902429	42.93572	12.44	3.13	5261	-0.56	155.32	40.35	0.29
7461601	296.29989	43.07131	13.43	2.90	4893	-0.46	50.17	82.46	0.14
7604896	290.9272605	43.23875	13.09	2.92	4878	0.06	99.38	72.13	0.16
7630743	297.9376695	43.28479	12.62	3.14	4786	0.07	166.91	86.71	0.13
7631194	298.05033	43.23317	11.82	2.68	4994	0.07	58.83	57.06	0.20
7831725	294.8964	43.52991	12.87	2.66	4985	0.07	39.10	35.81	0.32
7880664	287.7593895	43.68936	12.36	2.63	4802	0.07	39.26	99.11	0.12
7944142	284.869578	43.733161	7.82	2.80	5055	0.07	74.88	6.69	1.73
8052184	298.7172	43.85774	13.51	3.56	5196	-0.30	253.94	78.51	0.15
8409750	281.62728	44.41363	12.20	3.27	5245	-0.18	206.51	36.58	0.32
8649099	299.32878	44.79816	11.23	2.54	4845	-0.20	44.92	74.07	0.16
8914107	300.59514	45.15587	12.08	3.12	4910	-0.06	165.07	230.17	0.05
9091772	292.936899	45.41815	11.53	2.95	5026	0.07	115.53	48.25	0.24
9291830	295.97199	45.71479	11.02	2.56	5038	0.07	43.86	85.70	0.14
9479404	297.08928	46.03567	9.83	2.85	5191	0.21	77.41	10.02	1.16
9582089	289.24935	46.26023	12.22	2.45	4608	0.24	23.72	80.49	0.14
9612084	299.8694295	46.24609	11.76	3.05	5095	-0.06	78.60	**265.85	0.04
9771905	292.40451	46.5417	11.71	2.15	4393	0.16	11.47	**238.68	0.05
9906673	297.57587	46.76234	12.74	2.69	4937	-0.22	37.73	27.36	0.42
10203751	290.21211	47.202	11.96	2.58	4816	-0.08	35.69	13.18	0.88
10528911	289.28019	47.70018	12.06	2.39	4889	0.21	33.33	60.12	0.19
10854977	288.95117	48.22104	13.81	3.19	5193	-0.24	181.64	10.47	1.11
10858675	290.6682705	48.20462	12.24	2.84	4967	-0.08	87.12	24.31	0.48
10878851	298.14741	48.29483	13.21	2.44	4981	0.07	34.02	79.74	0.15
11298371	292.571829	49.03284	10.26	2.44	4989	0.07	35.28	59.76	0.19
11618859	295.67499	49.61104	13.77	3.64	5355	0.04	259.83	33.80	0.34
11753010	285.65682	49.90863	11.01	2.06	4303	0.14	14.03	89.70	0.13
12117138	294.895719	50.60238	12.50	2.53	4805	0.07	39.99	2.63	4.40